Absorption-spectroscopy In Tissue-simulating Materials - A Theoretical and Experimental-study of Photon Paths

Patterson, M. S; Andersson-Engels, Stefan; Wilson, B. C; Osei, E. K

Published in:
Applied Optics

DOI:
10.1364/AO.34.000022

1995

Absorption spectroscopy in tissue-simulating materials: a theoretical and experimental study of photon paths

Michael S. Patterson, Stefan Andersson-Engels, Brian C. Wilson, and Ernest K. Osei

A diffusion model of noninvasive absorption spectroscopy was used to determine how the change in signal resulting from a point absorber depends on the position of that absorber relative to the source and detector. This is equivalent to calculating the relative probability that a photon will visit a certain location in tissue before its detection. Experimental mapping of the point-target response in tissue-simulating materials confirmed the accuracy of the model. For steady-state spectroscopy a simple relation was derived between the mean depth visited by detected photons, the source–detector separation, and the optical penetration depth. It was also demonstrated theoretically that combining a pulsed source with time-gated detection provides additional control over the spatial distribution of the photon-visit probability.

Key words: Absorption spectroscopy, tissue optics, diffusion theory.

1. Introduction

In the past decade there has been increasing interest in the application of *in vivo* optical absorption spectroscopy to biomedical problems. It has been used to estimate the concentration of endogenous[1] and exogenous[2] chromophores in tissue and, in some cases, to differentiate their chemical state[3,4] (e.g., oxy- versus deoxy-hemoglobin). Typically, light is delivered to the tissue being studied through an optical fiber or fiber bundle. This light is multiply scattered within the tissue, and some fraction again reaches the surface where it may be collected with another fiber. Even for optically homogeneous tissues, the amount of light detected depends on not only the total absorption coefficient of all chromophores present in the tissue but also the source–detector geometry, the scattering properties of the tissue, and the index of refraction. Mathematical models have been developed that relate the detected signal to these quantities and that permit estimation of the true absorption coefficient.[5–9] These steady-state models have also been extended to time-dependent cases in which the source is pulsed[10] or sinusoidally modulated.[11]

Photons can traverse many different multiple-scattering paths between the source and detector and some paths are more likely than others. For example, paths lying close to the tissue surface are rare because photons are likely to be scattered out through the surface. Long paths that penetrate deep within the tissue are also unlikely because the probability of absorption is high. Therefore the probability that a given volume element of the tissue is visited by a photon before it is detected depends on the tissue optical properties and the source–detector geometry. Knowledge of the spatial distribution of visit probability is clinically important because it defines the effective volume of tissue from which information is obtained during *in vivo* spectroscopy. It also facilitates the interpretation of results when an absorption change is spatially localized rather than distributed throughout the tissue. Our goal here is to describe the spatial visit pattern mathematically and to confirm the results with measurements made in tissue-simulating media.

This problem was first addressed by Weiss *et al.*[12] who used a simple random-walk model of light propagation to derive approximate analytic expressions for the expected number of visits made by a photon to an arbitrary location before its detection on the surface.

M. S. Patterson and E. K. Osei are with the Hamilton Regional Cancer Centre and McMaster University, Hamilton, Ontario, Canada. S. Andersson-Engels is with the Lund Institute of Technology, Lund, Sweden. B. C. Wilson is with the Ontario Cancer Institute and Ontario Laser and Lightwave Research Centre, Toronto, Ontario, Canada.

Received 23 September 1993; revised manuscript received 15 July 1994.

0003-6935/95/010022-09$06.00/0.

They also calculated the mean and standard deviation of the depth visited by detected photons and the dependence of these parameters on the optical properties of the tissue and the source–detector separation. Although these authors presented no experimental confirmation of their predictions, they did show good agreement with the results of more sophisticated Monte Carlo simulations. In a recent paper Schotland *et al.*[13] used time-dependent diffusion theory to calculate an analogous quantity they called the photon hitting density. They illustrated the dependence of the hitting density on the source–detector geometry and the window used for time-gated detection. They did not address steady-state measurements nor were experiments performed. An experimental study was done by Cui *et al.*[14] who placed a source and detector on the surface of a turbid liquid and interposed a large opaque screen with a small aperture in the liquid. By measuring the detected signal as a function of aperture position, these investigators attempted a direct measurement of the time-resolved visit probability calculated by Weiss *et al.*[12] Whereas qualitative agreement with Weiss's predictions of mean depth was observed, the presence of the large opaque screen most likely perturbed the measurements, and no detailed mapping of the visit probability was performed.

The theoretical approach taken in this paper is somewhat different. Suppose we wish to know the relative probability that photons will visit a volume element dV before they reach the detector. If the absorption coefficient of the tissue within dV is increased by a small amount, the number of photons that reach the detector decreases. This decrease will be directly proportional to the visit probability. Therefore our approach is to calculate the response of the detector to a point-absorbing target as a function of the position of that target.

First, we consider the case of cw absorption spectroscopy. The diffusion approximation is used to derive expressions for the fluence rate at an arbitrary point in tissue and for the escape function (the probability that photons emitted at the arbitrary location escape the tissue and reach the detector). The product of the fluence rate and escape functions gives the information needed, i.e., the reduction in signal that would be observed because of a local perturbation in the absorption coefficient. We also consider the case of time-gated absorption spectroscopy in which the source is an infinitesimally short pulse and the detected signal is measured in the time domain. Here the relative visit probability also depends on the time delay between the source pulse and the observed signal. The time-dependent diffusion theory addresses this problem, but numerical integration is necessary to derive the spatial dependence of the relative visit probability.

The cw model was tested experimentally in a tissue-simulating liquid with known optical absorption and scattering properties. A direct test entails placing a small absorbing target within the medium and measuring the decrease in the detected signal as a function of target position. Because the target must be small enough to permit submillimeter resolution, the decrease in signal because of its presence would be too small to measure with precision. Instead a fluorescent target was used, and the fluorescence signal was measured as a function of target position. (As shown below, the model must be modified to account for the small difference in optical properties of the medium at the excitation and emission wavelengths.) We tested the model for two source–detector separations and two different values of the absorption coefficient by making detailed maps of the response to the point fluorescent target.

Experimental confirmation of the time-resolved model with this technique would be more difficult for two reasons. First, the detected signal in a small time window would be much smaller than the time-integrated signal, and a correspondingly longer measurement time would be required for an adequate signal-to-noise ratio. Second, the fluorescence lifetime of the target is comparable with the typical photon-migration time in the scattering medium, so that any time-resolved measurement would have to be corrected for this effect. For these reasons we did not directly test the expression for the time-resolved point target response.

Having tested the accuracy of the cw model, we used it to address the clinically important question: For noninvasive absorption spectroscopy, what is the average depth from which information is obtained? This depth can be calculated by numerical integration, and graphic results are presented that show its dependence on the scattering and absorption coefficients of the tissue. We also show that the average visit depth is highly correlated with a single descriptor of the tissue: the effective attenuation coefficient μ_{eff}. Finally, we consider the case of a pulsed source and show how the average visit depth can be varied by time gating the signal received by the detector.

2. Theory

The geometry of the general problem is illustrated in Fig. 1. Light is introduced at a single point (S) on the tissue, which is represented by a uniform half-space bound by the x–y plane. The tissue is characterized by the speed of light in the tissue c, the absorption coefficient μ_a, the scattering coefficient μ_s, and the mean cosine of the scattering angle g. In the framework of diffusion theory[15–17] these last two quantities are collapsed into the reduced (or transport) scattering coefficient, $\mu_s' = (1 - g)\mu_s$. Scattered light is collected by a point detector (D) situated on the tissue surface a distance r from the source. Considering a volume element dV at an arbitrary location indicated by P(ρ, θ, z) in cylindrical coordinates, we seek an expression for the reduction in signal observed at D for an incremental increase in μ_a within dV.

Let the photon fluence rate at P be denoted by $\phi(\mathbf{r}')$. The number of photons absorbed per unit

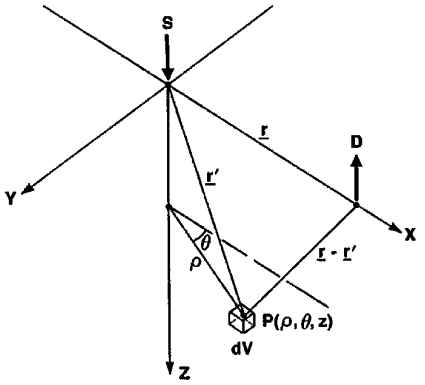

Fig. 1. Geometry for calculation of the relative visit probability in absorption spectroscopy. The light source (S) is a collimated pencil beam incident on the tissue at the origin, and a detector (D) is located at **r** on the tissue surface (the *x*–*y* plane). For the simple diffusion model it is assumed that all photons are isotropically scattered at a depth z_o on the *z* axis. As explained in the text, the fluence rate is assumed to be zero on a plane parallel to and above the tissue surface at $z = z_p$. The goal of the calculation is to determine the change in signal at the detector resulting from a perturbation in the absorption coefficient in d*V* near P(ρ, θ, *z*).

time in d*V* resulting from a small increment in absorption coefficient $\Delta\mu_a$ is $\Delta\mu_a\phi(\mathbf{r}')dV$. To calculate the reduction in photon number reaching the detector because of this loss in d*V*, we need to know the escape function $E(\mathbf{r}', \mathbf{r})$. If a photon is emitted at $\mathbf{r}'$, the probability of it reaching the surface at **r** (per unit area) is $E(\mathbf{r}', r)$, so the reflectance signal (photons per unit time per unit area) before the local perturbation $R(\mathbf{r})$ is changed by an amount

$$\Delta R(\mathbf{r}) = \Delta\mu_a\phi(\mathbf{r}')dVE(\mathbf{r}', \mathbf{r}). \quad (1)$$

We have implicitly assumed that the radiance (or angular photon flux) at $\mathbf{r}'$ is isotropic, because the escape function is calculated on the basis that all starting directions at $\mathbf{r}'$ are equally probable. This assumption is discussed in more detail below. Note also that the product $\phi(\mathbf{r}')E(\mathbf{r}', \mathbf{r})$ describes the spatial dependence of the response to an absorbing target. If the absorbing target is replaced by a fluorescent target, the resulting fluorescence signal (photons per unit time per unit area) $\Delta F(r, \lambda_x, \lambda_m)$ is given by

$$\Delta F(\mathbf{r}, \lambda_x, \lambda_m) = \Delta\mu_a\Phi\phi(\mathbf{r}', \lambda_x)dVE(\mathbf{r}', \mathbf{r}, \lambda_m), \quad (2)$$

where Φ is the fluorescence quantum yield at excitation wavelength λ_x and emission wavelength λ_m. Here the fluence rate and escape function have been written as explicit functions of wavelength to emphasize their dependence on the wavelength-dependent optical properties of the tissue. The spatial variation of the fluorescence signal is contained in the product $\phi(\mathbf{r}', \lambda_x)E(\mathbf{r}', \mathbf{r}, \lambda_m)$ similar to that for Eq. (1). Clearly, a model developed for calculating $\Delta R(\mathbf{r})$ can be tested by measurements of $\Delta F(\mathbf{r}, \lambda_x, \lambda_m)$ because the same mathematical form of the fluence rate and the escape function can be used. The experimental advantage is that ΔR represents a small change in a relatively large signal, whereas ΔF can be a small signal superimposed on a low background.

Equations (1) and (2) are generally true, in that we have invoked no approximate models of radiation transport. Monte Carlo simulation and other numerical methods[15–18] can be used to generate $\phi(\mathbf{r}')$ and $E(\mathbf{r}', \mathbf{r})$ for any given set of optical properties, but this approach provides little physical insight. At red and near-IR wavelengths for which $\mu_s' \gg \mu_a$ in tissue, the diffusion approximation to the radiation transport equation has been used successfully to describe the propagation of light in tissue.[16,18] We use this approach to generate analytic expressions for the fluence and the escape function, which are based on the well-known Green's function for diffusion in an infinite medium.[19] Note that for the diffusion approximation to be valid, the radiance must be close to isotropic. This is generally the case if $\mu_s' \gg \mu_a$ and provides justification for using the same escape function in Eqs. (1) and (2).

We start by writing the time-dependent diffusion equation for the photon fluence rate[15] as

$$\frac{1}{c}\frac{\partial}{\partial t}\phi(\mathbf{r}, t) - D\nabla^2\phi(\mathbf{r}, t) + \mu_a\phi(\mathbf{r}, t) = S(\mathbf{r}, t), \quad (3)$$

where $S(\mathbf{r}, t)$ is the photon source term (photons per unit volume per unit time) and the diffusion coefficient *D* is given by

$$D = \frac{1}{3(\mu_a + \mu_s')}. \quad (4)$$

We assume that all photons emitted by the source optical fiber enter the tissue at the origin of the coordinate system of Fig. 1 and that they are initially scattered at a depth z_o equal to the mean free path for effective isotropic scattering: $z_o = (\mu_s')^{-1}$. For the steady-state case therefore, $S(\mathbf{r}, t) = \delta(x, y, z - z_o)$. The solution of Eq. (3) requires specification of the boundary conditions. Although the exact boundary condition cannot be incorporated in diffusion theory, it has long been recognized[15,16] that a useful approximation for the case of a scattering medium bounded by air is to force the fluence rate to zero on an extrapolated boundary situated a distance z_e outside the actual physical boundary of the scattering medium. As discussed by Zhu *et al.*,[20] z_e depends on the average refractive index of the scattering medium. For the experimental conditions described below, the value of z_e calculated according to Farrell *et al.*[9] by the formula of Keijzer *et al.*[21] is $z_e = (5.91)D$. Because a real source of photons exists at a distance $z_e + z_o$ below the extrapolated boundary (i.e., at coordinate $z = z_o$), one can meet the zero-fluence-rate boundary condition by introducing a negative image source at $z_e + z_o$ above the extrapolated boundary (i.e., at $z = -z_o - 2z_e = z_p$). Within the scattering medium the fluence rate is the same as it would be in an infinite medium with this dipole source present. Using the steady-state, infinite medium solution to

Eq. (3), we can write the fluence at an arbitrary point $P(\rho, z)$ in tissue as

$$\phi(\rho, z) = \frac{1}{4\pi D}\left\{\frac{\exp[-\mu_{\text{eff}}[(z - z_o)^2 + \rho^2]^{1/2}\}}{[(z - z_o)^2 + \rho^2]^{1/2}} - \frac{\exp[-\mu_{\text{eff}}[(z - z_p)^2 + \rho^2]^{1/2}]}{[(z - z_p)^2 + \rho^2]^{1/2}}\right\}, \quad (5)$$

where μ_{eff}, the effective attenuation coefficient, is equal to $(\mu_a/D)^{1/2}$.

We now require an expression for the escape function $E(\rho, \theta, z, r)$. To derive this, we find first the fluence in the medium from a point source at (ρ, θ, z). One can do this by using the method of images as in Eq. (3). The escape function is given by the photon current across the boundary at $z = 0$, which, according to Fick's law,[15] is

$$\left(-D\frac{\mathrm{d}}{\mathrm{d}z}\phi\right)_{z=0}. \quad (6)$$

Evaluation of the derivative leads to the following expression for the escape function for a unit source at (ρ, θ, z):

$$E(\rho, \theta, z, r) = \frac{1}{4\pi}\left[\frac{z\exp(-\mu_{\text{eff}}k)}{k^2}\left(\mu_{\text{eff}} + \frac{1}{k}\right) - \frac{z_p\exp(-\mu_{\text{eff}}l)}{l^2}\left(\mu_{\text{eff}} + \frac{1}{l}\right)\right], \quad (7)$$

where k and l are the positive roots of

$$k^2 = (r - \rho\cos\theta)^2 + \rho^2\sin^2\theta + z^2, \quad (8)$$

$$l^2 = (r - \rho\cos\theta)^2 + \rho^2\sin^2\theta + z_p{}^2. \quad (9)$$

Substitution of Eqs. (5) and (7) into Eq. (1) or Eq. (2) yields the predicted response to a small absorbing or fluorescent target, respectively.

The use of time-resolved absorption spectroscopy can be approached in the same manner. In this case the observed quantity is $R(\mathbf{r}, t)$, the number of photons reaching the surface per unit time per unit area at distance r from the source at time t after application of an impulse source. Again we wish to calculate the change in $R(\mathbf{r}, t)$ resulting from an increment in μ_a in $\mathrm{d}V$ at $\mathbf{r}'$. Consider a time interval $\mathrm{d}t'$ at some time t' where $|\mathbf{r}'|/c < t' < t - |\mathbf{r} - \mathbf{r}'|/c$. The lower limit corresponds to the time at which light first reaches $\mathbf{r}'$, and the upper limit is the latest time at which light at $\mathbf{r}'$ could still reach $\mathbf{r}$ at time t. The number of photons absorbed in $\mathrm{d}V$ during $\mathrm{d}t'$ because of the absorption perturbation is $\Delta\mu_a\phi(\mathbf{r}', t')\mathrm{d}V\mathrm{d}t'$.

To relate this loss to the reduction in signal at time t, we need the time-resolved escape function $E(\mathbf{r}', \mathbf{r}, t - t')$, where $E(\mathbf{r}', \mathbf{r}, t - t')\mathrm{d}A\mathrm{d}t$ is the probability that a photon emitted at r' at time t' will reach the surface in the area element $\mathrm{d}A$ at $\mathbf{r}$ in the time interval $\mathrm{d}t$ at t. In parallel with Eq. (1) the reduction in the number of photons reaching the surface at $\mathbf{r}$ and t (per unit area per unit time) because of absorption in $\mathrm{d}t'$ at $\mathbf{r}'$ is

$$\Delta R(\mathbf{r}, t, t')\mathrm{d}t' = \Delta\mu_a\phi(\mathbf{r}', t')\mathrm{d}VE(\mathbf{r}', \mathbf{r}, t - t')\mathrm{d}t'. \quad (10)$$

To calculate the total loss from absorption perturbation, we must consider all possible times t' so that the total reduction in photon number $\Delta R(\mathbf{r}, t)$ is given by

$$\Delta R(\mathbf{r}, t) = \Delta\mu_a\mathrm{d}V\int_{|\mathbf{r}'|/c}^{t-|\mathbf{r}-\mathbf{r}'|/c}\phi(\mathbf{r}', t')E(\mathbf{r}', \mathbf{r}, t - t')\mathrm{d}t'. \quad (11)$$

Approximate expressions for the fluence rate and escape function, analogous to the steady-state versions in Eqs. (5) and (7), can be found by solving the time-dependent diffusion equation for an impulse source.[10] The final equations are

$$\phi(\rho, z, t') = c(4\pi Dc)^{-3/2}t'^{-3/2}\exp(-\mu_a ct') \times\left\{\exp\left[-\frac{(z - z_o)^2 + \rho^2}{4Dct'}\right] - \exp\left[-\frac{(z - z_p)^2 + \rho^2}{4Dct'}\right]\right\}, \quad (12)$$

$$E(\rho, \theta, z, r, t - t') = \frac{1}{2}(4\pi Dc)^{-3/2}(t - t')^{-5/2} \times\exp[-\mu_a c(t - t')] \times\left\{z\exp\left[-\frac{k^2}{4Dc(t - t')}\right] - z_p\exp\left[-\frac{l^2}{4Dc(t - t')}\right]\right\}. \quad (13)$$

Substitution of Eqs. (12) and (13) into Eq. (11) permits calculation of the spatial dependence of the response to a local absorber, although numerical techniques are necessary for evaluation of the convolution integral in Eq. (11).

3. Materials and Methods

As discussed above, the goal of the experiments was to confirm the predictions of Eqs. (2), (5), and (7) by measuring the detected fluorescence signal as a function of target position. The experimental setup is illustrated schematically in Fig. 2. The fluorescence excitation source was a Lexel Model 98 all-line argon-ion laser. The laser beam was expanded and passed through two interference filters to select the 488-nm line and to suppress any light at longer wavelengths. The light was then focused by a 50-mm focal-length lens into a 600-μm-core all-quartz optical fiber. The distal end of the fiber was polished flat and positioned on the surface of the tissue-simulating phantom. The power emitted by the fiber was kept at ~2 mW to minimize bleaching the fluorescent target.

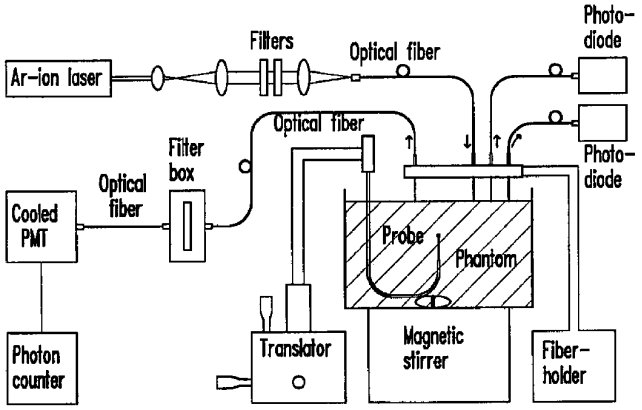

Fig. 2. Schematic diagram of the apparatus used to measure the signal resulting from the fluorescent target as a function of its position. PMT, photomultiplier tube.

The phantom consisted of ethylene glycol to which titanium dioxide particles and India ink were added to control the scattering and absorption coefficients, respectively. Other potential phantom materials such as lipid emulsions or aqueous suspensions of polystyrene microspheres were found to produce an unacceptably high-fluorescence background. Ethylene glycol was used as a carrier rather than water in an attempt to minimize settling of the titanium dioxide particles, which had a mean diameter of 0.5 μm. Although this was partially successful, we still had to provide gentle stirring of the phantom at all times to ensure a uniform particle distribution.

Once the phantom material was prepared with known optical properties (see below), it was poured into a 10 cm × 10 cm opaque container to a depth of 9 cm. The fluorescent target consisted of a poly(methyl methacrylate) (PMMA) cylinder of 0.4-mm length, 0.3-mm diameter, and 0.03-mm^3 volume, impregnated with the dye Nile Blue and mounted on a 200-μm-core optical fiber. This fluorescence-tipped optical fiber was designed originally as an interstitial fluence probe, and its construction was described in detail by Lilge *et al.*[22] Except for the last 2 cm at the target, the fiber was supported within a thin-walled stainless-steel tube fixed to a three-axis micropositioner that permitted translation of the target in the *x*, *y*, and *z* directions.

The fluorescent light from the target was detected through another flat cut-and-polished 600-μm quartz fiber positioned at a distance *r* from the source fiber and in contact with the phantom surface. The light was passed through a combination of cut-on and bandpass filters that rejected the excitation light and had maximum transmission at 575 nm, the peak of the fluorescence emission spectrum of Nile Blue in PMMA. This filtered light was detected by a cooled (−10 °C) photomultiplier tube (Hamamatsu R2228) operated in the single-photon counting mode. Pulses were amplified (PRA preamplifier Model 1763) and counted (PRA discriminator Model 1762 and PRA counter Model 1770) in the usual manner.

As shown in Fig. 2, two additional optical fibers were also placed in contact with the phantom and coupled to silicon photodiode radiometers (Photodyne 88XL). These detectors measured 488-nm light scattered from the phantom at arbitrary fixed positions. The signal from one detector was used to monitor changes in input laser power. The ratio of the two signals was monitored to ensure that no change in the optical properties of the phantom (for example, from settling) occurred during an experiment.

For each set of optical properties of the phantom and separation of the source and detector fibers, the response to the fluorescent target was mapped in two planes. One plane (the *x*–*z* plane in Fig. 1) contained the source and detector fibers, whereas the other was the perpendicular vertical plane halfway between the source and detector. For each plane, measurements were made by scanning the target in the *z* direction for a given *x*, *y* position from the greatest depth toward the surface. Immediately before and after each vertical scan the laser power was measured and adjusted if necessary, a background signal was measured with the target removed from the phantom, and a reference signal was recorded with the target at a depth of 2 mm halfway between the source and detector fibers. The background measurement permitted correction for light arising from sources other than the target, and the reference signal permitted correction for any target bleaching. (This amounted to at most 10% over the course of an experiment.) The signal from each target position was taken as the mean of three consecutive readings, each acquired over at least 20 s.

To determine the optical properties of the phantoms, we separately measured the absorption and transport scattering coefficients of suspensions of India ink in ethylene glycol and titanium dioxide in ethylene glycol. As stated above, the ink suspensions are expected to be mostly absorbing, so that μ_a of the phantom is fixed by the ink concentration. Similarly the TiO_2 suspensions are highly scattering so that μ_s' is determined by the TiO_2 particle concentration.

The measurement of the optical properties of India ink has been described in detail.[23] For the ink suspensions used in these experiments, the absorption coefficient of 1% ink in ethylene glycol was found to be 4.2 mm^{-1} at 488 nm and 3.5 mm^{-1} at 575 nm.

The optical properties of the titanium dioxide suspensions were measured by three different techniques:

(1) The diffuse reflectance and transmittance method combined with narrow-beam attenuation measurements as used for the ink samples.[23]

(2) An added absorber method described in detail elsewhere.[24]

(3) A frequency domain method described by Patterson *et al.*[11]

A summary of all the measurements of μ_s' for 1% TiO_2 suspensions at 488 and 575 nm is presented in Table 1. In the following analysis we used the mean

Table 1. Reduced (or Transport) Scattering Coefficient for 1-wt. % TiO_2 Particles in Ethylene Glycol Determined by Various Methods

Method	μ_s' (488 nm) (mm^{-1})	μ_s' (575 nm) (mm^{-1})
Added absorber	8.9	7.7
Reflectance/transmittance	10.5	9.0
Frequency domain	9.3	8.2
Mean	9.6	8.3

values $\mu_s' = 9.6\ mm^{-1}$ at 488 nm and $\mu_s' = 8.3\ mm^{-1}$ at 575 nm. The absorption coefficient of the suspension was found to be negligible compared with that of ink at the concentrations used to manufacture the phantoms. The index of refraction of the phantom was assumed to be 1.435, the value supplied by the manufacturer for pure ethylene glycol.

4. Experimental Results

Complete spatial maps of the fluorescent target response were obtained for the three sets of conditions listed in Table 2. As discussed above, these measurements are directly related to the relative photon-visit probability. The source–detector separation was either 6.6 or 9.6 mm, the transport scattering coefficient ranged from 0.73 to 0.87 mm^{-1}, and the absorption coefficient from 0.0044 to 0.016 mm^{-1}. These values are typical of soft tissues in the near-IR spectral region.[25] In Fig. 3 the experimental data are compared with the predictions of Eq. (2) generated with the values in Table 2. Note that the small difference in optical properties at the excitation and emission wavelengths has been accounted for. In generating the smooth curves in Fig. 3, two parameters were varied to give the best fit to the experimental data. First, for each data set (i.e., one panel in Fig. 3) an overall normalization was adjusted to give the best match for the entire family of curves. Second, because of the difficulty of indexing all the fibers to the liquid surface, and because the target has a finite volume and is not a true point target, an overall depth offset (see Table 2) was permitted in the z coordinate. This offset, which was typically 0.4 mm, was applied to the entire family of curves comprising a data set. None of the optical properties was adjusted in generating the comparisons shown in Fig. 3. The agreement, which is remarkably good in all measurement conditions and over signal amplitudes varying by greater than 2 orders of magnitude, demonstrates that the relative visit probability can be accurately calculated by the simple diffusion model.

Table 2. Experimental Conditions for Measurement of the Point Response Functions in Fig. 3[a]

Run	Fiber Separation (mm)	μ_s' (488 nm) (mm^{-1})	μ_a (488 nm) (mm^{-1})	μ_s' (575 nm) (mm^{-1})	μ_a (575 nm) (mm^{-1})	Offset (mm)
1	9.6	0.87	0.0053	0.75	0.0044	0.5 0.3
2	6.6	0.86	0.011	0.74	0.0088	0.8 0.6
3	9.6	0.85	0.016	0.73	0.013	−0.2 0.2

[a]The offset refers to the adjustment made in the z coordinate of the target to achieve the best fit, as described in the text. For each run the first offset was applied to the data acquired in the x–z plane and the second offset to data measured in the perpendicular plane midway between the source and detector.

5. Model Predictions and Discussion

Having established confidence in the diffusion model, we used it to address the following question: What is the average depth in tissue from which information is obtained during *in vivo* absorption spectroscopy and how does this depth depend on the tissue optical properties? The same problem was considered by Weiss *et al.*[12] using their random-walk model. For steady-state measurements the mean photon-visit depth for a source–detector separation of r, $\langle z \rangle_r$, is given by

$$\langle z \rangle_r = \frac{\int_V \phi(\rho, \theta, z) E(\rho, \theta, z, r) z \, dV}{\int_V \phi(\rho, \theta, z) E(\rho, \theta, z, r) \, dV}, \qquad (14)$$

where $\phi(\rho, \theta, z)$ and $E(\rho, \theta, z, r)$ are defined by Eqs. (5) and (7), respectively. We evaluated the integrals in Eq. (14) numerically for a wide range of tissue optical properties: $0.01\ mm^{-1} < \mu_a < 0.1\ mm^{-1}$ and $0.5\ mm^{-1} < \mu_s' < 5.0\ mm^{-1}$. In Fig. 4 the mean depth is plotted as lines of constant $\langle z \rangle_r$ in the space defined by μ_a and μ_s' for the case of $r = 10$ mm. As anticipated the largest values of $\langle z \rangle_r$ are found for low absorption and scattering coefficients, and an increase in either of these quantities causes the mean depth to decrease.

The shape of the constant $\langle z \rangle_r$ contours in Fig. 4 suggests that $\langle z \rangle_r$ might be correlated with a single-tissue descriptor, the effective attenuation coefficient μ_{eff}, or its reciprocal, the penetration depth δ. In Fig. 5 we replotted all the data used to generate Fig. 4 in the form of $\langle z \rangle_r$ versus $\delta^{1/2}$, and indeed all the points cluster near a straight line. This is also true for data generated for $r = 5$ mm and $r = 20$ mm. The lines shown in Fig. 5 were calculated by the empirical relationship $\langle z \rangle_r = (r\delta)^{1/2}/2$, which permits a reasonably accurate prediction of $\langle z \rangle_r$ from knowledge of r and δ alone. An identical functional relationship was derived by Weiss *et al.*,[12] although a different constant appears in the denominator of their expression. (This constant is either 1.59 or 1.74, depending on the interpretation of the absorption coefficient used by these authors.) Figure 5 demonstrates how the depth of tissue probed in noninvasive applications can be controlled by proper selection of the source–

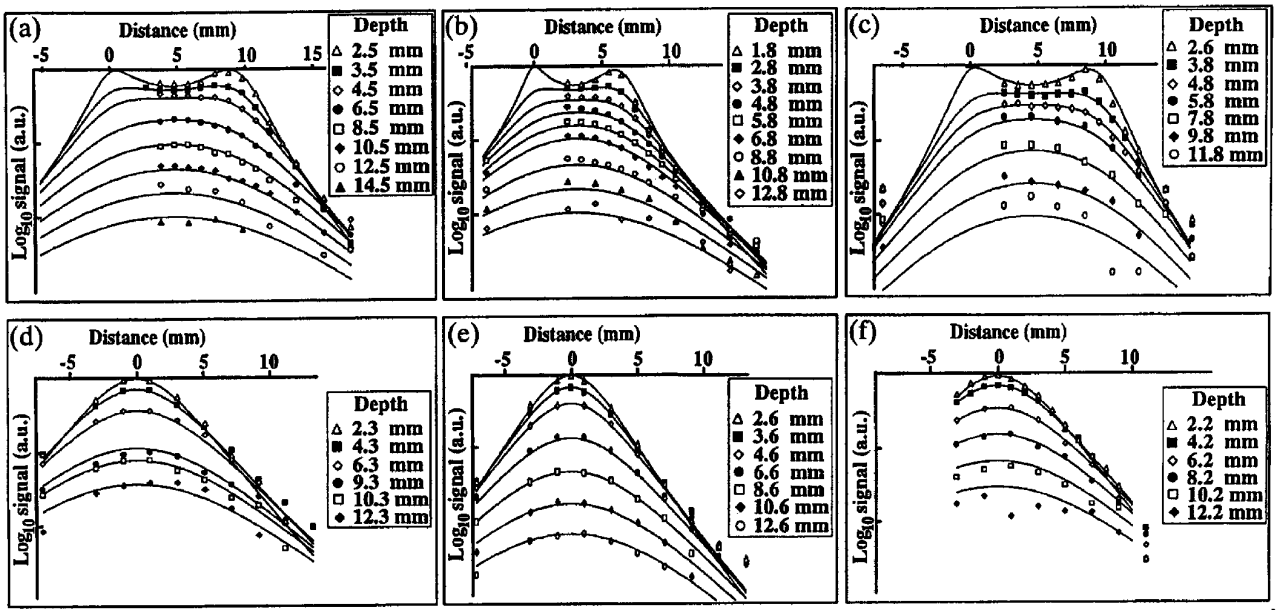

Fig. 3. Relative signal resulting from the fluorescent target as a function of its position. (a), (b), (c) Data acquired at different depths by scanning the target parallel to the x axis in the x–z plane (see Fig. 1). (d), (e), (f) Scans made parallel to the y axis at different depths in the plane midway between the source and detector. The optical properties of the scattering medium and source–detector separation are in Table 2. (a), (d) Run 1; (b), (e) run; 2; (c), (f) run 3. Note that each division on the ordinate scale corresponds to a factor of 10.

detector separation, although the consideration of other factors such as the signal-to-noise ratio may be necessary in practice.

For a fixed source–detector separation, control of the relative visit probability can be achieved with a pulsed source and time-gated detection. Clearly, photons that reach the detector at later times have traveled longer paths and are more likely to have penetrated deeper into the tissue. Calculation of $\langle z\rangle_{r,t}$, the mean depth of photon visitation for source–detector separation r and detection time t, is given by

$$\langle z\rangle_{r,t} = \frac{\int_V z\,dV \int_{|\mathbf{r}'|/c}^{t-|\mathbf{r}-\mathbf{r}'|/c} \phi(\mathbf{r}', t')E(\mathbf{r}', \mathbf{r}, t-t')dt'}{\int_V dV \int_{|\mathbf{r}'|/c}^{t-|\mathbf{r}-\mathbf{r}'|/c} \phi(\mathbf{r}', t')E(\mathbf{r}', \mathbf{r}, t-t')dt'}, \quad (15)$$

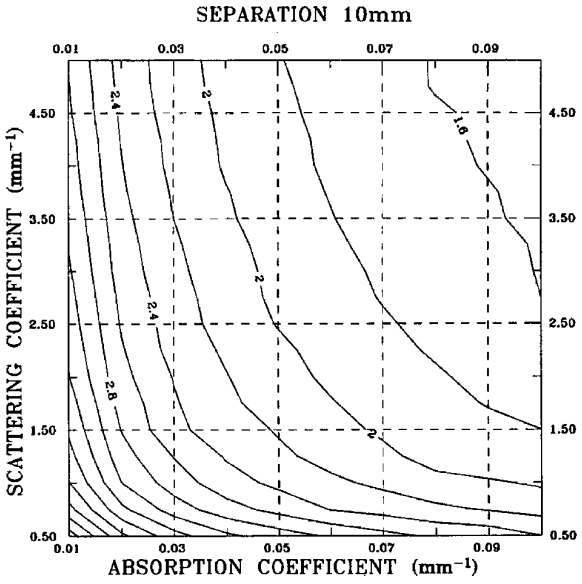

Fig. 4. Results of numerical calculation of the mean photon-visit depth during steady-state noninvasive absorption spectroscopy according to Eq. (14). Isodepth curves (in millimeters) are shown in the plane defined by the reduced scattering coefficient and absorption coefficient of the tissue. The contour interval is 0.2 mm, and the source–detector separation is 10 mm.

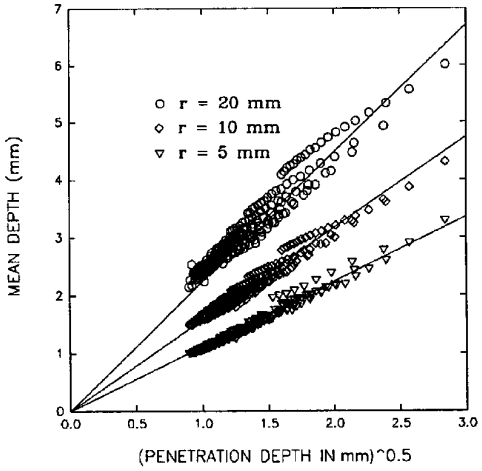

Fig. 5. Plots of the mean photon-visit depth during steady-state absorption spectroscopy versus the square root of the optical penetration depth in the tissue for three different source–detector separations. The points were obtained by the same sort of calculation used to generate Fig. 4 for three different source–detector separations. The lines are the empirical relaxation $\langle z\rangle_r = (r\delta)^{1/2}/2$.

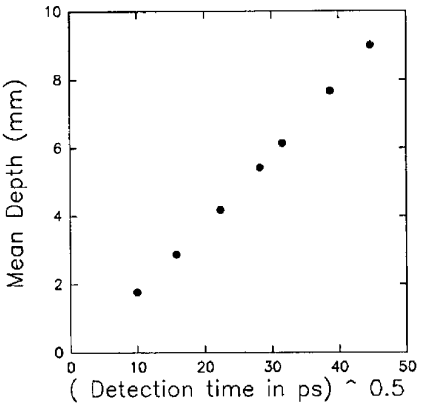

Fig. 6. Dependence of the mean photon-visit depth on the square root of the detection time when the source is an impulse and the detector is time gated. For this example, $\mu_s' = 1.0\ \text{mm}^{-1}$, $\mu_a = 0.01\ \text{mm}^{-1}$, $c = 0.214\ \text{mm ps}^{-1}$, and $r = 10$ mm.

where $\phi(r', t')$ and $E(\mathbf{r}', \mathbf{r}, t - t')$ are specified by Eqs. (12) and (13). As an example, we have calculated $\langle z \rangle_{r,t}$ for $r = 10$ mm, $\mu_a = 0.01\ \text{mm}^{-1}$, $\mu_s' = 1.0\ \text{mm}^{-1}$, and t ranging from 100 to 2000 ps. The results are plotted in Fig. 6 in the form $\langle z \rangle_{r,t}$ versus $t^{1/2}$, because, for a diffusive process, the mean distance traveled depends on the square root of time. (In the conditions in Fig. 6, the diffusion Green's function has been shown to represent accurately the fluence rate for a time of flight greater than 100 ps.[26]) The observed dependence of $\langle z \rangle_{r,t}$ on the square root of the detection time is indeed close to linear. By changing the detection time from 100 to 2000 ps, one can increase the mean depth from which information is obtained from 1.7 to 9.0 mm. By way of comparison, Fig. 5 shows that for the same geometry $\langle z \rangle_{10}$ is 3.6 mm in steady-state conditions. Thus time gating offers the potential for varying the depth of tissue probed with a single fixed source–detector combination. However, as shown by Weiss *et al.*,[12] the distribution of depths visited also broadens as the detection time is increased. We note as well that a number of groups[27–30] have demonstrated experimentally that time-gated control of the photon-visit probability can be used to enhance the spatial resolution of optical imaging in tissues.

6. Conclusions

We have developed a simple model of noninvasive absorption spectroscopy of homogeneous tissues for both steady-state and time-gated applications. The model was used to predict how the change in the detected diffuse reflectance signal measured on the tissue surface because of a local change in absorption depends on the location of that change relative to the source–detector combination. We showed that this is equivalent to calculating the relative probability that a photon will visit a given location before its detection. The accuracy of this model was demonstrated by direct measurement of the response to a small fluorescent target in tissue-simulating phantoms. For steady-state application a simple relation was derived between the mean photon-visit depth, the source–detector separation, and the optical penetration depth. It was also demonstrated that time-resolved techniques offer the additional capability of varying the volume of tissue interrogated during *in vivo* absorption spectroscopy. This model should be useful in clinical applications for which understanding the spatial dependence of the visit probability is required in choosing an appropriate detection geometry and in interpreting the results.

The authors are grateful to the Ontario Laser and Lightwave Research Centre and to the Swedish Research Council for Engineering Sciences for financial support of this research. Careful preparation of this manuscript by Donna Laking is also appreciated.

References

1. F. F. Jobsis, J. H. Keizer, J. C. LaManna, and M. Rosenthal, "Reflectance spectroscopy of cytochrome aa3 *in vivo*," J. Appl. Physiol. **43,** 858–872 (1977).
2. M. S. Patterson, B. C. Wilson, J. W. Feather, D. M. Burns, and W. Pushka, "The measurement of dihematoporphyrin ether concentration in tissue by reflectance spectrophotometry," Photochem. Photobiol. **46,** 337–343 (1987).
3. M. Cope and D. T. Delpy, "System for long-term measurement of cerebral blood and tissue oxygenation on newborn infants by near infrared transillumination," Med. Biol. Eng. Comput. **26,** 289–294 (1988).
4. B. Chance, S. Nioka, J. Kent, K. McCully, M. Fountain, R. Greenfeld, and G. Holtom, "Time resolved spectroscopy of hemoglobin and myoglobin in resting and ischemic muscle," Anal. Biochem. **174,** 698–707 (1988).
5. R. A. J. Groenhuis, H. A. Ferwerda, and J. J. Ten Bosch, "Scattering and absorption of turbid materials determined from reflection measurements. 1. Theory," Appl. Opt. **22,** 2456–2462 (1983).
6. R. F. Bonner, R. Nossal, S. Havlin, and G. H. Weiss, "Model for photon migration in turbid biological media," J. Opt. Soc. Am. A **4,** 423–432 (1987).
7. J. M. Schmitt, G. X. Zhou, E. C. Walker, and R. T. Wall, "Multilayer model of photon diffusion in skin," J. Opt. Soc. Am. A **7,** 2141–2153 (1990).
8. J. M. Steinke and A. P. Shepherd, "Diffuse reflectance of whole blood: model for a diverging light beam," IEEE Trans. Biomed. Eng. **BME-34,** 826–833 (1986).
9. T. J. Farrell, M. S. Patterson, and B. C. Wilson, "A diffusion theory model of spatially resolved, steady-state diffuse reflectance for the noninvasive determination of tissue optical properties *in vivo*," Med. Phys. **19,** 879–888 (1992).
10. M. S. Patterson, B. Chance, and B. C. Wilson, "Time resolved reflectance and transmittance for the noninvasive measurement of tissue optical properties," Appl. Opt. **28,** 2331–2336 (1989).
11. M. S. Patterson, J. D. Moulton, B. C. Wilson, K. W. Berndt, and J. R. Lakowicz, "Frequency-domain reflectance for the determination of the scattering and absorption properties of tissue," Appl. Opt. **30,** 4474–4476 (1991).
12. G. H. Weiss, R. Nossal, and R. F. Bonner, "Statistics of penetration depth of photons re-emitted from irradiated tissue," J. Mod. Opt. **36,** 349–359 (1989).
13. J. C. Shotland, J. C. Haselgrove, and J. S. Leigh, "Photon hitting density," Appl. Opt. **32,** 448–453 (1993).
14. W. Cui, N. Wang, and B. Chance, "Study of photon migration depths with time-resolved spectroscopy," Opt. Lett. **16,** 1632–1634 (1991).

15. J. J. Duderstadt and L. J. Hamilton, *Nuclear Reactor Analysis* (Wiley, New York, 1976).
16. A. Ishimaru, *Wave Propagation and Scattering in Random Media* (Academic, New York, 1978), Vol. 1.
17. H. C. van de Hulst, *Multiple Light Scattering Tables, Formulas and Applications* (Academic, New York, 1980).
18. M. S. Patterson, B. C. Wilson, and D. R. Wyman, "The propagation of optical radiation in tissue. I: Models of radiation transport and their application," Lasers Med. Sci. **6,** 155–168 (1990).
19. S. Chandrasekhar, "Stochastic problems in physics and astronomy," Rev. Mod. Phys. **15,** 1–88 (1943).
20. J. X. Zhu, D. J. Pine, and D. A. Weitz, "Internal reflection of diffusive light in random media," Phys. Rev. A **44,** 3948–3959 (1991).
21. M. Keijzer, W. M. Star, and P. R. Storchi, "Optical diffusion in layered media," Appl. Opt. **27,** 1820–1824 (1988).
22. L. Lilge, T. Haw, and B. C. Wilson, "Miniature isotropic optical fibre probes for quantitative light dosimetry in tissues," Phys. Med. Biol. **38,** 215–230 (1993).
23. S. J. Madsen, M. S. Patterson, and B. C. Wilson, "The use of India ink as an optical absorber in tissue-simulating phantoms," Phys. Med. Biol. **37,** 985–993 (1992).
24. B. C. Wilson, M. S. Patterson, and D. M. Burns, "The effect of photosensitizer concentration on the penetration depth of photoactivating light," Lasers Med. Sci. **1,** 235–244 (1986).
25. W. F. Cheong, S. A. Prahl, and A. J. Welch, "A review of the optical properties of biological tissues," IEEE J. Quantum Electron. **26,** 2166–2185 (1990).
26. J. D. Moulton, "Diffusion modelling of picosecond laser pulse propagation in turbid media," M. Eng. thesis (McMaster University, Hamilton, Ontario, Canada, 1990).
27. J. C. Hebden, R. A. Kruger, and K. S. Wong, "Time resolved imaging through a highly scattering medium," Appl. Opt. **30,** 788–794 (1991).
28. B. B. Das, K. M. Yoo, and R. R. Alfano, "Ultrafast time-gated imaging in thick tissues: a step toward optical mammography," Opt. Lett. **18,** 1092–1094 (1993).
29. R. Berg, O. Jarlman, and S. Svanberg, "Medical transillumination imaging using short-pulse diode lasers," Appl. Opt. **32,** 574–579 (1993).
30. E. M. Sevick, J. R. Lakowicz, H. Smacinski, K. Nowaczyk, and M. L. Johnson, "Frequency domain imaging of absorbers obscured by scattering," J. Photochem. Photobiol. B: Biol. **16,** 169–185 (1992).